Orient Academies

Noise Constrained Design Optimization of Road Edge Tactile Warnings via Coupled Tire and Road Acoustic Modeling

Ramon Dela Peña[1], Carlo Vergara[2], Miguel Santos[3]

Abstract

Roadway departure crashes remain a persistent contributor to severe injuries and fatalities, motivating infrastructure-based countermeasures that can operate independently of driver compliance. Shoulder profiling features that induce tactile and auditory cues are widely deployed because they can alert inattentive drivers with minimal operational cost. However, these features also radiate sound to the environment, creating an externality that becomes salient in residential corridors and in contexts with strict noise expectations. This paper develops a technical framework for designing road-edge profile geometries that preserve alerting efficacy while explicitly constraining community noise. The core contribution is a coupled tire–road contact and acoustic radiation model that maps profile geometry to both in-vehicle and far-field sound metrics through physically interpretable intermediate states, including contact force spectra, structural filtering, and radiation efficiency. We cast geometry selection as a robust multi-objective optimization problem under uncertainty in vehicle speed, tire type, suspension transfer characteristics, pavement temperature, and installation tolerances. The proposed formulation introduces a safety-relevant alerting constraint based on interior spectral energy in frequency bands associated with driver perception, and a community-impact constraint based on weighted exterior radiated power subject to propagation variability. We derive tractable surrogate structures enabling gradient-informed search over manufacturable profile parameterizations while enforcing smoothness and durability constraints. A validation protocol is described that emphasizes field-reproducible measurement harmonization between interior and exterior metrics. The resulting approach provides a principled pathway for agencies to tune tactile warning infrastructure to local noise sensitivity without sacrificing safety function.

[1] *Nueva Ecija University of Science and Technology, Department of Construction Technology, Maharlika Highway, Cabanatuan City 3100, Philippines*

[2] *Cebu Technological University, Department of Infrastructure Engineering, M.J. Cuenco Avenue, Cebu City 6000, Philippines*

[3] *University of Eastern Philippines, Department of Structural Engineering Technology, Catarman Heritage Road, Catarman, Northern Samar 6400, Philippines*

Contents

1 Introduction 1
2 Background and Problem Formulation 4
3 Coupled Vibro-Acoustic Modeling 7
4 Robust Multi-Objective Design Optimization 10
5 Experimental Protocols and Validation Strategy 12
6 Discussion and Implications 13
7 Conclusion 14
References 15

1. Introduction

Run-off-road events combine high prevalence with high consequence because they often involve loss of control, fixed-object impacts, or rollover mechanisms [1]. The underlying causal chain is frequently mundane: transient distraction, drowsiness, or a brief steering error that would otherwise be recoverable if detected early enough. Road-edge tactile warning infrastructure aims to shorten the time-to-detection by converting lateral drift into a multimodal cue that is difficult to ignore. A distinctive property of this intervention is that it couples mechanical interaction at the tire–pavement interface to both vehicle-borne vibration and airborne acoustic radiation. The same interaction that produces an interior cue can

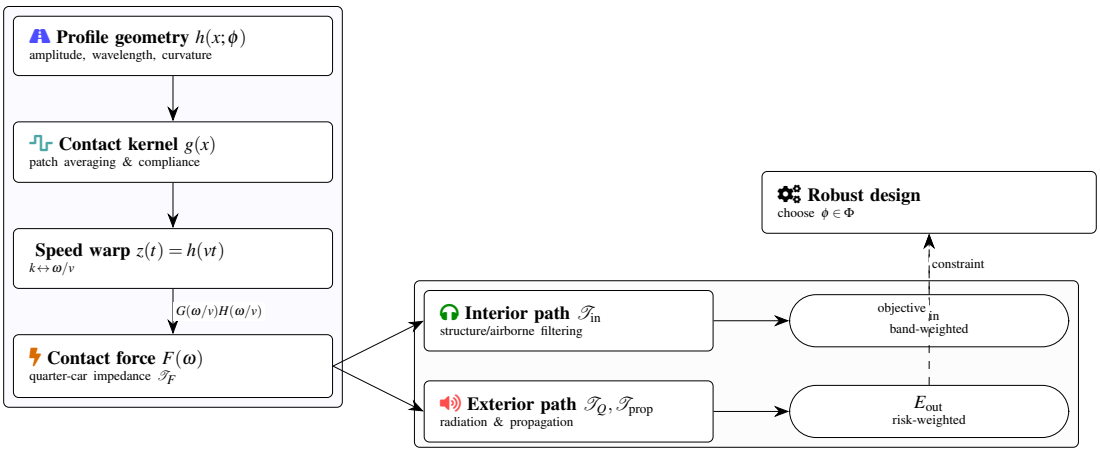

Figure 1. End-to-end mapping from road-edge geometry to coupled interior and exterior outcomes. The spatial profile is contact-filtered and speed-warped into temporal excitation, generating force spectra that propagate through distinct interior and exterior transfer paths to produce the metrics used in robust design.

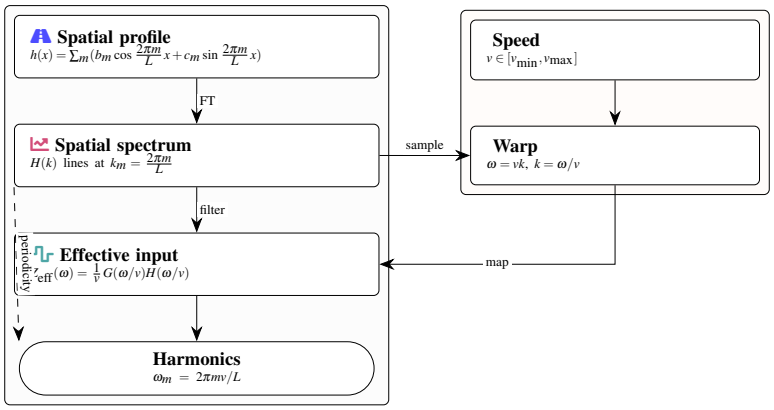

Figure 2. Spatial-to-temporal spectral mapping enabling frequency-aware geometry tuning. Discrete components in $H(k)$ shift with speed via $\omega = vk$, while contact filtering $G(\cdot)$ suppresses fine spatial detail; the surviving components determine harmonic locations and the spectral structure experienced by the vehicle and environment.

also radiate sound outward, and the latter can be experienced as intrusive in quiet environments even when the safety function is satisfied. The resulting tension is not simply political or perceptual; it is rooted in the physics of contact excitation, the transfer properties of the vehicle body and cabin, and the radiation of sound from spatially distributed sources near the roadway surface. Because these elements depend on geometry, speed, and fleet composition, it is not sufficient to treat external noise as an afterthought or as a fixed penalty applied to a standard design.

The engineering challenge is to shape the profile so that it creates a reliable alert within the cabin while limiting radiated exterior noise [2]. This is a multi-domain problem in which small changes to wavelength, amplitude, groove curvature, and spacing can shift the energy distribution across frequencies that are filtered differently by the suspension and the cabin than by outdoor propagation. Moreover, the operational environment introduces uncertainty. Vehicles vary widely in tire stiffness, tread pattern, wheelbase, damping, and cabin insulation. Speeds can span a broad range, and pavement conditions modulate the contact mechanics through temperature-dependent stiffness and surface compliance. Construction tolerances and wear further perturb the realized geometry. A design that looks optimal for a single nominal vehicle at a single speed may fail to produce adequate interior salience for a substantial portion of the fleet, or it may generate unexpected exterior tonal components that carry farther than predicted.

Existing design practice often relies on a combination of standardized geometric templates and empirical knowledge accumulated through field experience. Such practice has clear pragmatic advantages but leaves performance tradeoffs underdetermined in the face of conflicting objectives and local constraints. In noise-sensitive contexts, agencies sometimes avoid installation altogether or accept repeated complaint cycles that lead to partial removal, which in turn can degrade safety consistency along a corridor [3]. A more systematic approach would treat the geometry as a decision variable in a model that explicitly represents both safety-relevant alerting and external radiated noise, and that can be calibrated to local

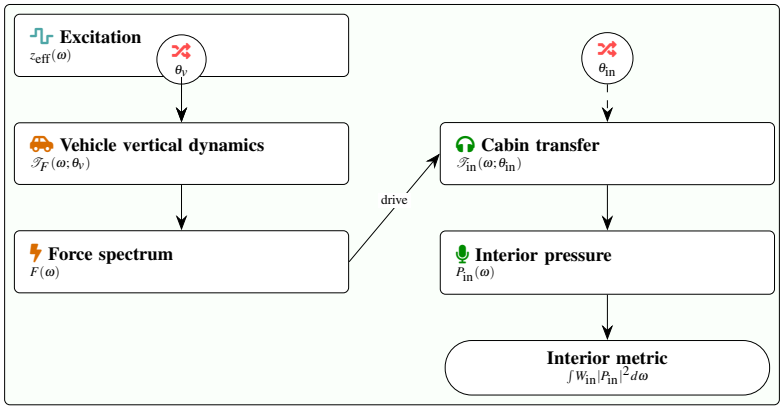

Figure 3. Reduced interior path emphasizing differential filtering and uncertainty entry points. Geometry-induced excitation drives a vehicle dynamics block that shapes force spectra, which are then filtered by an uncertain cabin transfer function; salience is assessed through a band-weighted interior energy metric (optionally relative to baseline).

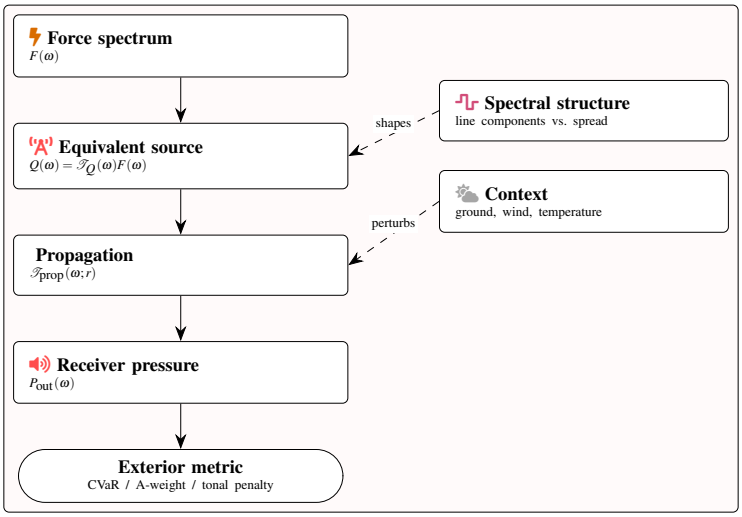

Figure 4. Exterior path abstraction for community impact assessment. Force fluctuations drive an equivalent radiating source whose spectral structure can be tonal or distributed depending on geometry; propagation then modulates bands through distance and ground/atmospheric effects, and the metric can be chosen to emphasize tail events and/or narrowband prominence.

fleet and roadway characteristics.

A notable field study conducted by Sallam et al. (2025) indicated that sinusoidal shoulder profiles can yield lower exterior noise levels than a traditional design while still producing adequate in-vehicle level increases, highlighting that geometric shaping can materially shift the safety–noise tradeoff rather than merely scaling both outputs together [4]. That observation motivates a broader and more general question: what design principles govern the mapping from profile geometry to the joint distribution of interior and exterior acoustic outcomes across uncertain operating conditions, and how can those principles be operationalized into a robust optimization procedure that yields manufacturable geometries with predictable performance?

This paper addresses that question by developing a coupled vibro-acoustic modeling and optimization framework for road-edge profiling. The thesis is that profile geometries should be designed by targeting the spectral structure of contact excitation in a way that leverages differential filtering: the vehicle path from contact force to cabin sound is shaped by suspension and body transfer functions, whereas the path to far-field radiation is shaped by source coherence, radiation efficiency, and atmospheric and ground interaction. By explicitly modeling these two paths, one can identify geometry families that are intrinsically biased toward interior salience and exterior suppression. The technical contribution is a unified forward model linking geometry parameters to both in-cabin and exterior metrics, a robust multi-objective formulation accounting for key uncertainties, and a surrogate-enabled solver strategy that remains tractable for agency-relevant parameterizations and constraints. The intent is not to replace field testing but to provide a design stage tool that narrows the candidate space, rationalizes tradeoffs, and supports context-specific tuning [5].

The remainder of the paper proceeds as follows. The next section formalizes the design problem and introduces

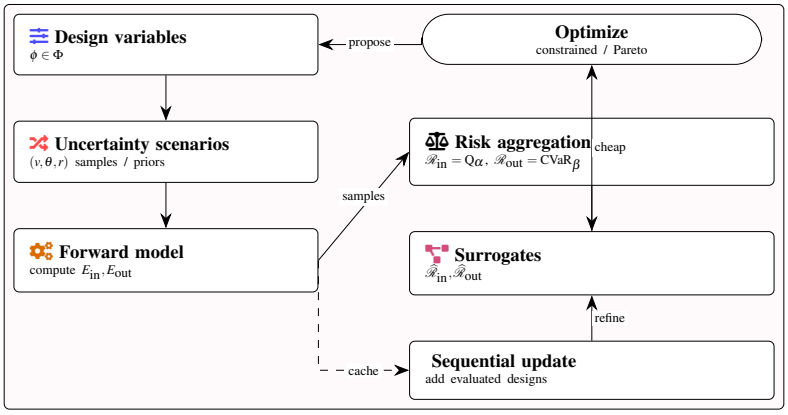

Figure 5. Surrogate-enabled robust optimization workflow. Designs are evaluated over uncertainty scenarios, aggregated through quantile and tail-risk measures, and emulated by surrogates to enable efficient constrained search; periodic updates re-anchor the surrogate with newly evaluated designs.

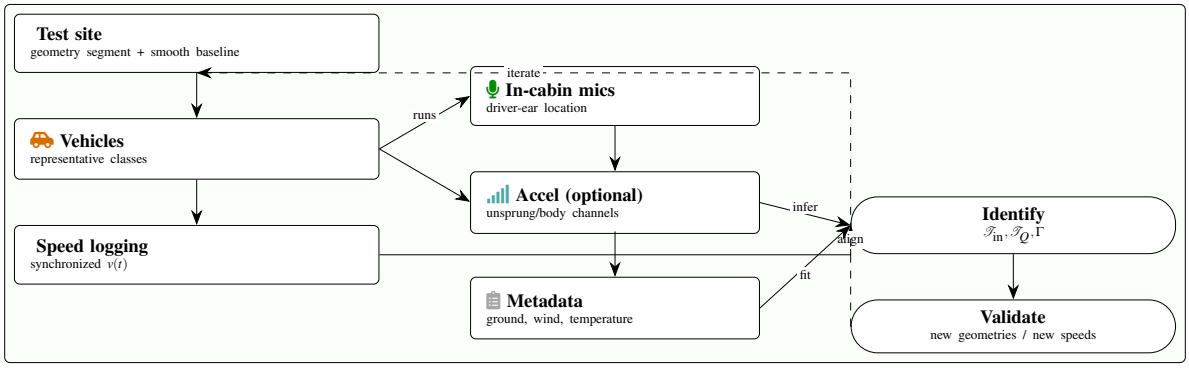

Figure 6. Field measurement harmonization and validation strategy aligned with the reduced-order model. Interior and exterior recordings are collected with synchronized speed traces (and optional vibration channels) to preserve geometry-induced spectral structure, support identification of effective transfer/propagation parameters, and enable validation on geometries and speeds withheld from calibration.

the geometry parameterization and performance metrics. The subsequent section develops the coupled tire–road contact, structural transmission, and acoustic radiation models, emphasizing frequency-domain structure and uncertainty pathways. The optimization section then presents a robust formulation with manufacturability and durability constraints and describes a surrogate-assisted approach for efficient search. A validation strategy section outlines measurement harmonization and calibration considerations to ensure the model can be grounded in field data. The discussion section interprets the design implications, including how geometry choices redistribute spectral energy and how robust solutions differ from nominal optima. The paper concludes by summarizing contributions and identifying technical directions for future refinement.

2. Background and Problem Formulation

A road-edge profile can be interpreted as a spatial modulation of the tire support surface that converts lateral motion into a time-varying vertical displacement at the contact patch. When a vehicle traverses the profile at speed, the spatial structure is transformed into temporal excitation [6]. The resulting contact forces feed into vehicle structural dynamics, producing vibration and airborne sound inside the cabin through structure-borne and airborne pathways. Simultaneously, the interaction generates sound that radiates into the environment through mechanisms that include vibrating tire sidewalls and tread blocks, pressure fluctuations in the grooves, and radiation from the near-surface source distribution. From a design perspective, it is convenient to treat the profile as the primary controllable input and to define objective and constraint functions that map the profile to interior alerting efficacy and exterior noise impact.

Let the profile height relative to a nominal shoulder plane be represented by a function $h(x)$ defined along the travel direction coordinate x. In practice, the profile is realized by grooves, indentations, or raised features, but for modeling it can be approximated as a continuous function with bounded curvature and amplitude, supplemented by constraints that prevent sharp edges associated with accelerated wear or maintenance difficulty. The vehicle travels with speed v, so the tire experiences an effective vertical displacement input $z(t) = h(vt)$ along a trajectory that depends on lateral offset. The contact patch has finite length, so the tire does not respond to a pointwise height but rather to a filtered version of $h(x)$ that

Symbol / quantity	Meaning	Domain / notes
$h(x)$	Profile height relative to nominal shoulder plane	Spatial coordinate x along travel direction
$z(t) = h(vt)$	Effective vertical displacement input at contact patch	Time-domain excitation induced by geometry and speed
v	Vehicle speed	Random variable over corridor-dependent distribution
k	Spatial frequency	Related to temporal frequency by $f = vk/(2\pi)$
$H(k)$	Spatial Fourier transform of $h(x)$	Design-controlled spectral content of profile
$G(k)$	Spatial contact kernel spectrum	Encodes patch averaging and tire compliance

Table 1. Key spatial and temporal quantities linking road-edge profile geometry to tire excitation.

Metric / function	Definition sketch	Interpretation
$E_{\text{in}}(h; v, \theta)$	$\int W_{\text{in}}(\omega)\lvert P_{\text{in}}(\omega)\rvert^2 d\omega$	Band-weighted interior acoustic energy for alerting
$E_{\text{out}}(h; v, \theta, r)$	$\int W_{\text{out}}(\omega)\lvert P_{\text{out}}(\omega)\rvert^2 d\omega$	Band-weighted exterior energy related to community impact
$W_{\text{in}}(\omega)$	Perceptual / band weighting for cabin sound	Emphasizes frequencies relevant for driver salience
$W_{\text{out}}(\omega)$	Regulatory / annoyance weighting for exterior sound	Can incorporate A-weighting and tonal penalties
$p_{\text{in}}(t)$, $P_{\text{in}}(\omega)$	Interior pressure and its spectrum at driver ear	Increment over smooth shoulder forms alerting signal
$p_{\text{out}}(t)$, $P_{\text{out}}(\omega)$	Exterior pressure and its spectrum at reference receiver	Used for pass-by and equivalent level assessments

Table 2. Interior and exterior acoustic metrics and weighting functions used in the performance evaluation.

reflects the averaging effect of the patch and the compliance distribution.

A key design variable is the spectral content of the resulting contact force. Because $z(t)$ is a time-warped version of $h(x)$, the temporal frequency content scales with speed [7]. A purely periodic spatial waveform with spatial frequency k produces a temporal frequency $f = vk/(2\pi)$. Therefore, geometric parameters such as wavelength and spacing effectively target specific temporal bands at typical speeds. The cabin response tends to have resonant structures and frequency-dependent attenuation, meaning that placing energy in bands with high cabin sensitivity can yield stronger perceptual cues for the same contact force magnitude. Exterior radiation, on the other hand, may be stronger in other bands due to tire radiation efficiency and propagation characteristics. This motivates a frequency-aware approach rather than a purely time-domain amplitude approach.

We define two performance metrics. The interior alerting metric should reflect not only overall sound pressure level but also spectral distribution in bands relevant to driver perception and annoyance balance, recognizing that the purpose is salience rather than comfort. The exterior metric should represent community impact, often related to maximum pass-by level, equivalent continuous level over events, or a weighted measure that penalizes tonal components. Because policy and community response vary, the model should be flexible, allowing the exterior metric to be defined as a weighted norm over frequency and direction, potentially incorporating propagation effects.

Denote the interior acoustic pressure at the driver ear location by $p_{\text{in}}(t)$ and the exterior pressure at a reference location by $p_{\text{out}}(t)$. In the frequency domain, let $P_{\text{in}}(\omega)$ and $P_{\text{out}}(\omega)$ be their Fourier transforms. Define band-weighted energies

$$E_{\text{in}}(h; v, \theta) = \int_0^\infty W_{\text{in}}(\omega)\,\lvert P_{\text{in}}(\omega; h, v, \theta)\rvert^2\, d\omega \quad \text{and} \tag{1}$$

$$E_{\text{out}}(h; v, \theta, r) = \int_0^\infty W_{\text{out}}(\omega)\,\lvert P_{\text{out}}(\omega; h, v, \theta, r)\rvert^2\, d\omega, \tag{2}$$

where θ denotes uncertain vehicle and tire parameters and r denotes propagation and receiver geometry parameters. The weighting functions W_{in} and W_{out} can encode perceptual weighting, regulatory emphasis, or agency priorities. In practice, the interior metric may also include a baseline subtraction relative to smooth shoulder travel, focusing on incremental alerting rather than absolute cabin noise.

The design problem is to choose $h(x)$ within a manufac-

Element	Symbol / form	Role in formulation	Typical behavior
Interior risk measure	$\rho_{\text{in}}(E_{\text{in}})$	Enforces alerting reliability under uncertainty	Often lower quantile of interior energy
Exterior risk measure	$\rho_{\text{out}}(E_{\text{out}})$	Captures noise impact and high-noise tails	Expectation or CVaR over uncertain conditions
Regularization	$\Omega(h)$ or $\Omega(\phi)$	Penalizes curvature, promotes durability	Suppresses high spatial harmonics
Admissible set	$\mathscr{H}$ or Φ	Restricts geometry to manufacturable family	Encodes basis choice and feasibility
Geometry constraints	$A_{\min}, A_{\max}, S_{\max}, C_{\max}$	Limit amplitude, slope, curvature	Avoids excessive wear and sharp features
Tradeoff parameter	λ	Balances exterior impact and regularization	Tuned to agency priorities

Table 3. Core components of the optimization problem linking safety-relevant alerting and exterior noise impact.

Parameter	Description	Influence on profile behavior
a_0	Mean offset of $h(x)$ over one period	Controls average recess or elevation of the profile
a_m (or b_m, c_m)	Amplitude of mth harmonic component	Shapes depth and sharpness of repeated features
ψ_m (phase)	Phase of mth harmonic	Adjusts alignment and local waveform asymmetry
L	Spatial period of the base waveform	Sets fundamental excitation frequency via $f_1 = v/L$
M	Number of harmonics retained	Controls geometric richness and potential tonal content

Table 4. Fourier-based parameterization of road-edge profile geometry over a spatial period L.

turable family to minimize expected exterior impact while ensuring interior alerting exceeds a threshold with high reliability. Because uncertainty is central, we define a robust constraint: the interior metric should exceed a minimum level for a specified quantile over uncertainty. Similarly, the exterior metric may be minimized in expectation, in a worst-case sense, or using a risk measure that penalizes high-noise tails. A general formulation is

$$\begin{aligned} \min_{h\in\mathscr{H}} \quad & \rho_{\text{out}}\big(E_{\text{out}}(h;v,\theta,r)\big) + \lambda\,\Omega(h) \\ \text{s.t.} \quad & \rho_{\text{in}}\big(E_{\text{in}}(h;v,\theta)\big) \geq E_{\min}, \\ & A_{\min} \leq h(x) \leq A_{\max}, \quad \forall x, \\ & |h'(x)| \leq S_{\max}, \quad |h''(x)| \leq C_{\max}, \quad \forall x[8]. \end{aligned} \tag{3}$$

where $\mathscr{H}$ is the admissible set, $\Omega(h)$ is a regularization reflecting durability or maintenance, λ is a tradeoff parameter, and ρ_{out} and ρ_{in} are risk measures such as expectation, conditional value-at-risk, or quantiles. The slope and curvature constraints formalize geometric smoothness, and amplitude bounds prevent excessive structural excitation or rapid wear.

A continuous function space is conceptually useful but computationally unwieldy. We therefore parameterize $h(x)$ using a low-dimensional family that can represent common groove patterns and smooth waveforms while remaining manufacturable. One convenient choice is a periodic base waveform over a spatial period L with a finite Fourier series and a phase parameter capturing alignment relative to travel direction. Another is a spline representation with knot spacing set by construction capabilities. For a periodic waveform, we can write

$$h(x;\phi) = a_0 + \sum_{m=1}^{M} a_m \cos\left([9]\frac{2\pi m}{L}x + \psi_m\right) \tag{4}$$

$$\text{with} \quad \phi = (a_0, a_1, \ldots, a_M, \psi_1, \ldots, \psi_M, L). \tag{5}$$

and impose constraints on coefficients that ensure bounded slope and curvature. The phase terms allow the design to represent sinusoidal-like, trapezoidal-like, or more complex shapes without introducing discontinuities. A groove-based design can be approximated by choosing higher harmonics, but smoothness constraints will suppress unrealistic sharp edges. Alternatively, a spline representation can capture localized grooves with rounded edges, and periodic repetition can be added by construction.

The uncertainty variables require explicit modeling choices. Vehicle speed v can be treated as a random variable supported on a corridor-specific distribution. Tire stiffness, damping, and contact patch length can be modeled as random vari-

Symbol / block	Description	Uncertainty representation	Notes
v	Vehicle speed along profile	Random variable with corridor-specific distribution	Shifts temporal location of harmonics
θ_v	Quarter-car and tire parameters	Random across vehicle classes and loading states	Controls contact force filtering
θ_{in}	Cabin and body transfer parameters	Random across fleet and interior configurations	Affects interior sensitivity bands
θ_Q	Radiation efficiency parameters	Random due to tire and wheel-well variability	Maps structural response to acoustic source strength
θ_r	Propagation and receiver parameters	Random due to ground, atmosphere, and geometry	Impacts far-field exterior levels

Table 5. Principal sources of uncertainty in vehicle, tire, and propagation properties within the modeling framework.

Operator	Maps	Physical pathway	Key features
$G(\cdot)$ and $H(\cdot)$	Profile $h(x)$ to $Z_{\text{eff}}(\omega)$	Contact patch averaging and spatial-to-temporal mapping	Speed-dependent sampling of spatial spectrum
$\mathscr{T}_F(\omega)$	Z_{eff} to $F(\omega)$	Unsprung and sprung mass dynamics	Resonances at wheel-hop and body modes
$\mathscr{T}_{\text{in}}(\omega)$	$F(\omega)$ to $P_{\text{in}}(\omega)$	Structure-borne and airborne interior transmission	Modal peaks shaped by cabin acoustics
$\mathscr{T}_Q(\omega)$	$F(\omega)$ to $Q(\omega)$	Conversion to equivalent acoustic source	Captures tire sidewall and tread radiation
$\mathscr{T}_{\text{prop}}(\omega)$	$Q(\omega)$ to $P_{\text{out}}(\omega)$	Outdoor propagation and ground interaction	Includes spreading, absorption, and reflections

Table 6. Sequence of transfer operators composing the forward vibro-acoustic model from geometry to interior and exterior sound.

ables conditioned on vehicle class [10]. The suspension and cabin transfer functions can be represented by uncertain parameters of a reduced-order model. Propagation uncertainties include receiver distance, ground impedance variation, and atmospheric absorption variability. The formulation is designed to accommodate these uncertainties without locking into a single fleet.

The remainder of the paper develops a forward model for P_{in} and P_{out} given ϕ and uncertainty, and then describes how to solve the resulting optimization problem efficiently. The guiding principle is to exploit the structured mapping from spatial geometry to temporal excitation and to keep intermediate quantities interpretable for calibration and sensitivity analysis.

3. Coupled Vibro-Acoustic Modeling

The forward model decomposes the mapping from geometry to sound into a sequence of operators: a geometry-to-contact excitation operator, a contact-to-vehicle structural response operator, a structural-to-cabin acoustic operator for the interior path, and a contact/structural-to-radiation operator for the exterior path. While a fully resolved simulation involving finite element tire models and boundary element acoustics could in principle capture detailed phenomena, such an approach is generally too expensive and too sensitive to unmeasured parameters for iterative design at the agency level. Instead, we develop a reduced-order model that preserves the spectral and scaling properties most relevant to geometry selection and uncertainty propagation.

The geometry-to-contact excitation mapping begins with the effective displacement input at the contact patch. A tire contact patch of length ℓ averages the road profile over a spatial window, and the tire carcass compliance further filters high spatial frequencies [11]. Let $g(x)$ be an effective contact kernel normalized to unit integral that represents this spatial averaging and compliance. The effective displacement input

Quantity	Definition	Typical choice	Design purpose
$\mathscr{R}_{\text{in}}(\phi)$	$\text{Quantile}_{\alpha}(E_{\text{in}})$	$\alpha \approx 0.1$ for 90% reliability	Ensures robust interior alerting across fleet
$\mathscr{R}_{\text{out}}(\phi)$	$\text{CVaR}_{\beta}(E_{\text{out}})$	$\beta \approx 0.9$ for upper-tail control	Limits high-noise events that drive complaints
$E_{\min}$	Minimum acceptable interior energy	Mapped to detectable in-cabin level increment	Defines safety constraint threshold
λ	Weight on regularization $\Omega(\phi)$	Selected via sensitivity or policy study	Balances smoothness/durability with noise goals
$\Omega(\phi)$	Curvature or harmonic penalty	$\int_0^L (h''(x;\phi))^2 dx$ or similar	Discourages aggressive, wear-prone geometries

Table 7. Risk measures and auxiliary quantities used in the robust multi-objective optimization formulation.

Component	Interior measurement focus	Exterior measurement focus
Microphone / sensor placement	Near driver ear with fixed cabin configuration	Standardized roadside receiver height and offset
Reference segment	Smooth shoulder baseline for incremental metrics	Baseline pass-by levels without profiling
Speed logging	High-resolution synchronized speed trace	Verification of speed stationarity during passes
Background conditions	Engine, HVAC, and wind-control protocols	Wind screening and ambient noise documentation
Receiver geometry	Cabin seat position and posture consistency	Multiple receiver distances / heights for propagation calibration
Vehicle fleet selection	Representative classes for interior transfer diversity	Overlap with dominant sources of community exposure

Table 8. Key elements of experimental protocols for calibrating and validating the reduced-order model.

is

$$z_{\text{eff}}(t) = \int_{-\infty}^{\infty} g(\xi)\, h(vt - \xi)\, d\xi. \tag{6}$$

In the frequency domain, if $H(k)$ is the spatial Fourier transform of $h(x)$ and $G(k)$ that of $g(x)$, then the temporal Fourier transform of $z_{\text{eff}}(t)$ satisfies a frequency-warp relationship. For a vehicle traveling at speed v, the temporal frequency ω corresponds to spatial frequency $k = \omega/v$, leading to

$$Z_{\text{eff}}(\omega) = \frac{1}{v} G\Big(\frac{\omega}{v}\Big) H\Big(\frac{\omega}{v}\Big). \tag{7}$$

This expression makes the role of geometry explicit: the spatial spectrum of the profile is sampled along a speed-dependent mapping. High spatial frequencies are attenuated by G, which captures the tendency of the patch and compliance to smooth sharp details. Because G depends on tire pressure, load, and construction, it is a natural pathway for uncertainty.

The effective displacement drives contact force through an impedance that includes tire stiffness, damping, and dynamic effects from wheel hop. A simplified but informative model is to represent the vertical dynamics of the unsprung mass as a second-order system driven by z_{eff}. Let m_u be effective unsprung mass, k_t tire stiffness, c_t tire damping, and let $y(t)$ be the vertical displacement of the wheel center relative to an inertial frame. The tire deflection is $y(t) - z_{\text{eff}}(t)$, and the contact force can be approximated as

$$F(t) = k_t\big(y(t) - z_{\text{eff}}(t)\big) + c_t\big(\dot{y}(t) - \dot{z}_{\text{eff}}(t)\big). \tag{8}$$

The wheel center displacement is influenced by suspension coupling to the sprung mass [12]. A reduced quarter-car model introduces sprung mass m_s, suspension stiffness k_s, and damping c_s. In the frequency domain, the transfer from Z_{eff} to F can be written as

$$F(\omega) = \mathscr{T}_F(\omega;\theta_v)\, Z_{\text{eff}}(\omega), \tag{9}$$

where $\mathscr{T}_F$ is a complex transfer function determined by vehicle parameters $\theta_v = (m_u, m_s, k_t, c_t, k_s, c_s)$. The explicit form can be derived by solving the coupled second-order system, yielding a rational function in ω with resonances corresponding to wheel hop and body modes. The reduced model is not intended to predict absolute forces for every vehicle but to capture the frequency shaping and the dependence on key parameters that vary across the fleet.

Design lever	Expected interior effect	Expected exterior effect
Fundamental wavelength L	Shifts harmonic frequencies relative to cabin modes	Shifts tonal bands relative to propagation-efficient ranges
Harmonic content (number and amplitudes)	Controls sharpness and spectral richness of alerting cue	Influences tonal prominence versus broadband radiation
Amplitude bounds on $h(x)$	Adjusts overall excitation strength and vibration levels	Sets upper limit on radiated sound and structural loading
Smoothness / curvature control	Moderates high-frequency interior content	Reduces excitation of high-frequency radiation mechanisms
Speed distribution in design	Targets robustness over operating speeds	Avoids unexpected peaks at rarely considered speeds
Fleet composition assumptions	Balances alerting for well-insulated vehicles	Limits noise for more transmissive vehicle classes

Table 9. Qualitative implications of geometry and context choices for the balance between interior alerting and exterior noise.

The interior path is modeled as a mapping from contact force to cabin sound pressure at the driver ear. Two dominant pathways are commonly recognized: structure-borne vibration transmitted through suspension and body panels that then radiate inside the cabin, and airborne noise generated near the wheel well that enters through openings or transmits through panels. A reduced representation can combine these pathways into an effective transfer function from contact force to interior pressure:

$$P_{\text{in}}(\omega) = \mathscr{T}_{\text{in}}(\omega;\theta_{\text{in}})\,F(\omega) + P_{\text{base}}(\omega), \tag{10}$$

where $\mathscr{T}_{\text{in}}$ is an uncertain transfer function capturing structural and acoustic filtering, θ_{in} are its parameters, and P_{base} represents background cabin noise from engine, wind, and road texture. In design for alerting, the relevant quantity is often the incremental pressure relative to baseline, so the model can focus on the additional contribution from the profile. Because P_{base} is not controlled by the profile, it enters primarily through the perceptual contrast ratio, and thus it can be accounted for by requiring a minimum increment in band-weighted energy or a minimum signal-to-noise ratio.

A practical parameterization of $\mathscr{T}_{\text{in}}$ is a sum of resonant filters reflecting dominant cabin and body modes. For example,

$$\mathscr{T}_{\text{in}}(\omega;\theta_{\text{in}}) = \sum_{j=1}^{J} \frac{\alpha_j \omega^2}{\omega_j^2 - \omega^2 + \mathrm{i}2\zeta_j\omega_j\omega} \exp(-\mathrm{i}\omega\tau_j), \tag{11}$$

where ω_j are modal frequencies, ζ_j are damping ratios, α_j are gain factors capturing coupling strength, and τ_j are effective delays representing phase lags across the structure [13]. This representation is flexible enough to fit measured interior transfer functions while remaining low-dimensional. Uncertainty arises because different vehicles have different modal properties and coupling strengths, and even within a vehicle, occupancy and cargo can shift modal frequencies.

The exterior path requires representing the radiation of sound into the environment. While tire–road noise is a complex phenomenon, for geometry comparison it is often sufficient to treat the dominant radiating sources as distributed near the contact patch and wheel well, driven by contact force fluctuations and associated structural vibrations. A reduced approach is to model an equivalent acoustic source strength $Q(\omega)$ proportional to a filtered version of contact force and, optionally, to tire structural response. We write

$$Q(\omega) = \mathscr{T}_Q(\omega;\theta_Q)\,F(\omega), \tag{12}$$

where $\mathscr{T}_Q$ captures conversion from force to volume velocity or dipole strength. The far-field pressure at a receiver can then be approximated by a propagation operator:

$$P_{\text{out}}(\omega;r) = \mathscr{T}_{\text{prop}}(\omega;r,\theta_r)\,Q(\omega), \tag{13}$$

where $\mathscr{T}_{\text{prop}}$ includes spherical spreading, ground reflection, atmospheric absorption, and receiver directivity effects. A simple model uses [14]

$$\mathscr{T}_{\text{prop}}(\omega;r,\theta_r) = \frac{\exp(-\mathrm{i}\omega r/c)}{4\pi r}\,\Gamma(\omega;\theta_r), \tag{14}$$

where c is sound speed and Γ is a complex factor representing ground and barrier effects. For design, the exact spatial detail may be less important than ensuring that exterior spectral energy is reduced in bands that dominate annoyance and that propagate efficiently.

The coupling between geometry and exterior noise is not solely through amplitude; coherence matters. Profiles with sharp periodicity can produce narrowband tonal components that carry farther and are perceived as more intrusive. Smooth or multi-frequency profiles can spread energy over frequency, reducing tonal prominence even if total energy is similar. To capture this, the model should preserve the spectral peaks induced by periodicity. The earlier mapping from spatial spectrum to temporal spectrum accomplishes this: if $h(x)$ is periodic with period L, then $H(k)$ has line components at harmonics of $2\pi/L$, leading to spectral lines in $Z_{\text{eff}}(\omega)$ at $\omega = 2\pi mv/L$. These lines can appear in both interior

and exterior sound, but their relative prominence depends on the transfer functions. Therefore, geometry selection can aim to place harmonics in interior-favorable regions while suppressing harmonics that align with exterior-sensitive or propagation-efficient bands.

The forward model can be consolidated into a single expression that maps spatial geometry to interior and exterior pressures: [15]

$$P_{\text{in}}(\omega) = \mathscr{T}_{\text{in}}(\omega;\theta_{\text{in}})\,\mathscr{T}_F(\omega;\theta_v)\,\frac{1}{v}\,G\Big(\frac{\omega}{v}\Big)\,H\Big(\frac{\omega}{v}\Big), \tag{15}$$

(16)

$$\begin{aligned} P_{\text{out}}(\omega;r) = {} & \mathscr{T}_{\text{prop}}(\omega;r,\theta_r)\,\mathscr{T}_Q(\omega;\theta_Q) \\ & \times \mathscr{T}_F(\omega;\theta_v)\,\frac{1}{v}\,G\Big(\frac{\omega}{v}\Big) \\ & \times H\Big(\frac{\omega}{v}\Big). \end{aligned} \tag{17}$$

This structure highlights a key design lever: $H(\omega/v)$ is the only component directly controlled by geometry. The remaining factors represent uncertain filters. Robust design thus becomes a problem of choosing H such that, across uncertainty, the product yields sufficient interior energy while keeping exterior energy low. Because the filters differ between interior and exterior, there is an opportunity to exploit differential shaping.

To connect this to the parameter vector ϕ, we compute $H(k;\phi)$ from the chosen basis representation. For the Fourier series parameterization of $h(x)$, H is sparse with coefficients linked to a_m and ψ_m. For a spline or rounded-groove parameterization, H can be computed numerically [16]. This enables evaluation of the performance metrics E_{in} and E_{out} by integrating over frequency with weights. In practice, the integrals are approximated over a finite band of interest, and the weights can include perceptual equal-loudness curves or policy-driven emphasis.

A subtle but important modeling issue is the relationship between sound level and driver alerting. Interior noise increases are often used as proxies for alerting, but salience depends on temporal structure, onset rate, and coupling with vibration. The present framework focuses on acoustic pressure because it is measurable and often used in standards, but the model can be extended by defining a multimodal alerting metric combining vibration at the steering wheel or seat with cabin sound. In the reduced-order setting, vibration can be linked to the same contact force through a transfer function $\mathscr{T}_{\text{vib}}(\omega)$, and the alerting metric can be a weighted sum of band energies. The optimization framework presented later remains applicable with such an extension.

The final element needed for robust optimization is a representation of uncertainty. We treat the uncertain parameters $\theta = (\theta_v, \theta_{\text{in}}, \theta_Q, \theta_r)$ and speed v as random variables with a joint distribution that can be constructed from fleet composition and environmental priors. Because full distributions may be unavailable, we also consider ambiguity sets defined by bounds and moments, enabling distributionally robust formulations. The forward model is sufficiently low-dimensional that Monte Carlo sampling over uncertainty can be used during calibration, while optimization can rely on surrogate approximations to reduce computational burden.

4. Robust Multi-Objective Design Optimization

The design objective is to suppress exterior noise impact without sacrificing interior alerting [17]. Because these goals conflict, the problem is inherently multi-objective. In practice, decision makers may prefer solutions that satisfy a minimum alerting constraint and then minimize exterior noise, or they may prefer to explore a Pareto frontier and choose a design based on context. The optimization framework should therefore support both constrained and tradeoff representations. Here we focus on a constrained formulation emphasizing safety assurance, while also describing how to compute Pareto sets.

Let ϕ denote the finite-dimensional geometry parameters defining $h(x;\phi)$, with admissible set Φ incorporating manufacturability and durability constraints. For each uncertainty realization (v,θ,r) we compute interior and exterior energies $E_{\text{in}}(\phi;v,\theta)$ and $E_{\text{out}}(\phi;v,\theta,r)$. We then define risk measures. For interior alerting, a natural requirement is that alerting exceed a threshold for most conditions. This can be expressed using a lower quantile:

$$\mathscr{R}_{\text{in}}(\phi) = \text{Quantile}_{\alpha}\big(E_{\text{in}}(\phi;v,\theta)\big), \tag{18}$$

where α is a small probability level such as 0.1, meaning that at least 90% of conditions achieve at least $\mathscr{R}_{\text{in}}$. The constraint is $\mathscr{R}_{\text{in}}(\phi) \geq E_{\min}$. For exterior noise, one may wish to limit not only mean levels but also high-noise tail events that drive complaints [18]. A conditional value-at-risk measure is suitable:

$$\mathscr{R}_{\text{out}}(\phi) = \text{CVaR}_{\beta}\big(E_{\text{out}}(\phi;v,\theta,r)\big), \tag{19}$$

where β is a high tail level such as 0.9, capturing the expected value in the worst 10% of cases. This makes the design conservative with respect to noise extremes without requiring strict worst-case optimization, which can be overly pessimistic given model uncertainty.

The resulting optimization is

$$\min_{\phi\in\Phi} \quad \mathscr{R}_{\text{out}}(\phi) + \lambda\,\Omega(\phi) \tag{20}$$

$$\text{subject to} \quad \mathscr{R}_{\text{in}}(\phi) \geq E_{\min}. \tag{21}$$

The regularization $\Omega(\phi)$ accounts for durability, drainage, and maintenance considerations that are difficult to express purely through slope and curvature bounds. For example, large curvature can concentrate stress and accelerate degradation. In

a Fourier parameterization, a curvature penalty corresponds to penalizing high harmonics because curvature scales with $(m/L)^2$. One can define

$$\Omega(\phi) = \int_0^L \left(h''(x;\phi)\right)^2 dx, \tag{22}$$

which is analytically tractable for Fourier series and encourages smooth waveforms [19]. This penalty also indirectly reduces high-frequency excitation that may be less useful for alerting and more likely to generate exterior broadband radiation.

A practical constraint set Φ includes amplitude and geometric feasibility:

$$A_{\min} \le h(x;\phi) \le A_{\max} \quad \text{and} \quad |h'(x;\phi)| \le S_{\max} \quad \text{for all } x, \tag{23}$$

and can also include a minimum feature width to avoid clogging and to support pavement integrity. In the Fourier basis, enforcing pointwise constraints can be done by sampling x on a fine grid and applying inequality constraints, which is acceptable given the low dimensionality. For spline representations, constraints can be enforced at knots and by bounding derivative control variables.

Computational tractability hinges on evaluating the risk measures efficiently. Direct Monte Carlo estimation within an optimization loop can be expensive, particularly because evaluating E_{in} and E_{out} involves frequency-domain integrals and possibly propagation models. However, the forward model has a compositional structure that allows efficient evaluation once transfer function parameters are specified. The main cost arises from sampling uncertainty and from integrating over frequency. To address this, we propose surrogate modeling in the design space combined with structured sampling in uncertainty space [20].

The surrogate strategy treats ϕ as the input and approximates $\mathscr{R}_{\text{in}}(\phi)$ and $\mathscr{R}_{\text{out}}(\phi)$ with smooth emulators. A Gaussian process surrogate is attractive for low-dimensional ϕ, but polynomial chaos or radial basis surrogates may be more stable for larger design spaces. Because the risk measures involve quantiles and CVaR, which can introduce non-smoothness in finite-sample estimates, it is useful to approximate the full distribution of E_{in} and E_{out} for each ϕ by moment models or by parametric distributions fitted to sampled realizations. A pragmatic approach is to sample a fixed set of uncertainty scenarios $\{(v_s, \theta_s, r_s)\}_{s=1}^{S}$ using quasi-Monte Carlo sequences, compute $E_{\text{in}}(\phi)$ and $E_{\text{out}}(\phi)$ for each scenario, and then compute empirical risk measures. The mapping from ϕ to the vector of scenario outcomes can be approximated by a surrogate, and the risk measures can be computed from the surrogate outputs at negligible incremental cost.

The design exploration proceeds iteratively. An initial space-filling design over Φ is generated, and for each design point the scenario outcomes are computed. Surrogates are fitted. Candidate designs are proposed by solving the surrogate-based optimization, with interior constraints enforced either directly or through a penalty method that discourages violations. New candidate designs are then evaluated using the true forward model, added to the training set, and the surrogates are updated. This sequential design reduces the number of expensive forward evaluations while converging toward robust optima.

A key advantage of the forward model structure is that, for a given uncertainty scenario, the mapping from ϕ to E_{in} and E_{out} is differentiable when $h(x;\phi)$ is smooth. This enables gradient-based optimization [21]. Differentiation can be carried out analytically for the Fourier parameterization because $H(k;\phi)$ depends linearly on coefficients. In the frequency domain, the band energy is a quadratic form in H, enabling explicit gradients. For instance, consider the interior energy for a fixed scenario:

$$E_{\text{in}}(\phi) = \int_0^\infty W_{\text{in}}(\omega) \left| \mathscr{K}_{\text{in}}(\omega) H\left(\frac{\omega}{v};\phi\right)\right|^2 d\omega, \tag{24}$$

where $\mathscr{K}_{\text{in}}(\omega)$ collects all factors independent of H. If H is linear in coefficients a_m and ψ_m, then E_{in} can be expressed as a quadratic function in these coefficients, up to the nonlinearity introduced by phases. By reparameterizing the Fourier series in terms of sine and cosine coefficients, the dependence becomes linear:

$$h(x) = a_0 + \sum_{m=1}^{M} \left(b_m \cos\left(\frac{2\pi m}{L}x\right) + c_m \sin\left(\frac{2\pi m}{L}x\right)\right), \tag{25}$$

with $\phi = (a_0, b_1, \ldots, b_M, c_1, \ldots, c_M, L)$. Then H has coefficients proportional to b_m and c_m, and energies become quadratic. This yields efficient gradient and even Hessian computations, enabling second-order optimization methods. The periodicity parameter L introduces nonlinearity because it shifts spectral line locations, but it is one scalar, and gradients can be computed by differentiating the mapping $\omega \mapsto \omega/v$ relative to L in the discrete frequency approximation.

Robust constraints based on quantiles are more challenging because quantiles of nonlinear functions are not smooth [22]. A common approach is to replace quantile constraints with smooth approximations using the log-sum-exp function or to enforce chance constraints using a scenario approximation. In a scenario approximation, one chooses S scenarios and enforces $E_{\text{in}}(\phi; v_s, \theta_s) \ge E_{\min}$ for all but a small number of scenarios, effectively controlling violation probability. This yields a set of deterministic constraints that can be handled by nonlinear programming. Because we avoid enumerated lists, we describe the scenario relaxation in continuous terms: one introduces slack variables representing violations and penalizes them in the objective, thereby encouraging satisfaction across scenarios while retaining feasibility during early iterations.

For exterior noise, CVaR can be computed as the solution of an auxiliary optimization problem:

$$\mathrm{CVaR}_\beta(X) = \min_\eta \left(\eta + \frac{1}{1-\beta}\,\mathbb{E}\left[(X-\eta)_+\right]\right), \tag{26}$$

where $(\cdot)_+$ is the positive part and η is a threshold. In a scenario setting, the expectation becomes an average over scenarios, and the positive part can be represented with smooth approximations or with auxiliary variables and inequality constraints. This makes CVaR amenable to gradient-based methods even when the underlying distribution is approximated empirically.

A central modeling decision is how to encode exterior noise sensitivity. If the metric is based on A-weighted level, then $W_{\text{out}}(\omega)$ can be chosen accordingly. If tonal noise is particularly undesirable, W_{out} can include a penalty on narrowband peaks. One way to incorporate tonal penalties without discrete peak detection is to penalize spectral sparsity by adding a convex function of the normalized spectrum, encouraging flatter spectra [23]. For example, one may add a term proportional to the integral of the squared spectrum relative to its mean, which increases when energy concentrates in narrow bands. Because the design controls harmonic structure, such a penalty can discourage overly periodic designs that generate pronounced tones.

To interpret solutions, it is useful to compute the Pareto frontier between $\mathscr{R}_{\text{out}}$ and $\mathscr{R}_{\text{in}}$. This can be done by varying $E_{\min}$ or by using a weighted sum objective. The resulting frontier can reveal whether small sacrifices in alerting robustness yield large gains in noise reduction or vice versa. Such information supports context-based decisions, such as more conservative alerting in high-speed rural corridors and stricter noise constraints in residential corridors.

The optimization is ultimately only as credible as the calibration of transfer functions and uncertainty models. Therefore, the next section describes a validation strategy emphasizing measurement alignment, parameter identification, and cross-vehicle generalization, ensuring that the model can be used as a design tool rather than a purely theoretical construct.

5. Experimental Protocols and Validation Strategy

A reduced-order model intended for design must be tied to measurement procedures that can be executed reproducibly in the field. The principal challenge is that interior and exterior sound levels are influenced by many confounders, including background noise, wind, surface texture variations, and transient vehicle states. If calibration data are inconsistent or poorly controlled, the identified transfer functions may absorb confounders, reducing predictive validity when applied to new geometries or contexts [24]. The validation strategy described here aims to separate the geometry-induced component from uncontrolled variability and to fit transfer functions that generalize across vehicle classes.

The first step is to define measurement conditions that provide a clear mapping to the model inputs. The model assumes a relationship between spatial geometry and temporal excitation via speed, so accurate speed measurement is essential. In practice, speed can vary during a pass, and even small variations can smear spectral lines for periodic geometries. Therefore, field runs should include high-resolution speed logging synchronized with audio. If constant-speed operation is difficult, the model can be extended to handle nonstationary speed by using time-frequency analysis, but for calibration it is preferable to maintain speed stability within a narrow tolerance.

For interior sound, microphones should be placed near the driver ear location, and the vehicle should be operated with consistent window and ventilation settings to reduce variability in cabin acoustics. Background noise should be recorded over a smooth shoulder segment under similar conditions to establish a baseline spectrum. Because the design objective concerns incremental alerting, the primary interior calibration quantity is the transfer from contact force to incremental interior pressure [25]. Direct force measurement at the contact patch is difficult in field settings, but one can approximate the force spectrum using accelerometers on the unsprung mass combined with a dynamic model, or one can treat the force as a latent variable and estimate an effective transfer directly from geometry to interior pressure by exploiting known $H(\omega/v)$ structure. The latter approach can work well when geometry is periodic and has strong harmonic content, because the input spectrum is known up to amplitude scaling by the contact kernel and tire stiffness.

For exterior sound, the receiver location should be specified relative to the roadway edge, and ground conditions should be documented because ground impedance affects propagation. A pass-by procedure that isolates vehicle-by-vehicle contributions is preferred over long-term ambient measurements, because the objective is to capture the incremental noise generated by the profile during traversal events. Microphone height and distance should be consistent, and wind screens should be used to reduce wind noise. The propagation operator in the model can be simplified if the receiver is in the acoustic far field relative to the source region, but for near-road receivers, ground reflection and interference can cause frequency-dependent cancellations and amplifications. Therefore, calibration should include multiple receiver distances and heights when feasible, allowing identification of $\Gamma(\omega;\theta_r)$ parameters.

A central concern is fleet heterogeneity [26]. The model includes uncertain parameters to represent differences across vehicles, but calibration must provide data to inform these distributions. One strategy is to collect data across representative vehicle classes, such as passenger cars, pickup trucks, and SUVs, using a small number of vehicles per class. The reduced transfer functions can then be fitted per vehicle and analyzed statistically to derive priors for modal frequencies and coupling gains. A particularly informative calibration quantity is the ratio of interior to exterior spectral energy for the same traversal, because it partially cancels uncertainties in the contact force amplitude. If a geometry produces similar force spectra across vehicles but yields different interior/exterior ratios, that difference is attributable to transfer

functions rather than input, and it can be used to refine the uncertainty model.

Parameter identification can be framed as an inverse problem. For each vehicle and measurement condition, the observed interior and exterior spectra are used to fit $\mathscr{T}_{\text{in}}$ and $\mathscr{T}_Q$ parameters. Because the model is linear in frequency domain, one can fit the magnitude and phase of transfer functions using regularized least squares. For example, let the predicted spectrum be $\hat{P}_{\text{in}}(\omega;\theta_{\text{in}}) = \mathscr{T}_{\text{in}}(\omega;\theta_{\text{in}})\,\hat{F}(\omega)$, where $\hat{F}$ is an estimated force spectrum derived from geometry and a nominal contact kernel. Then identification minimizes

$$J_{\text{in}}(\theta_{\text{in}}) = \int_{\omega_1}^{\omega_2} \left| [27]P_{\text{in,obs}}(\omega) - \hat{P}_{\text{in}}(\omega;\theta_{\text{in}}) \right|^2 d\omega + \mu \int_{\omega_1}^{\omega_2} \left| \frac{d^2}{d\omega^2} \mathscr{T}_{\text{in}}(\omega;\theta_{\text{in}}) \right|^2 d\omega. \tag{27}$$

where the second term enforces smoothness of the transfer function to avoid overfitting noise. Similar identification can be applied to the exterior path. When direct force estimation is unreliable, a joint identification can be performed where $\hat{F}$ is treated as a latent spectrum constrained by the geometry mapping and contact kernel, and interior and exterior observations jointly inform it. The joint approach leverages the fact that both interior and exterior responses share the same contact excitation [28].

Validation should be performed on geometries not used for calibration. A credible validation includes predicting the relative ranking of candidate geometries in terms of exterior noise under constraints on interior alerting. It also includes predicting how performance changes with speed, since speed dependence is central to the geometry-to-frequency mapping. The model should capture the shift of harmonic peaks with speed for periodic geometries and the associated changes in weighted energies. If the model fails to capture these shifts, it indicates that either the contact kernel is speed-dependent in a way not captured, or that nonlinearity in contact mechanics is significant, requiring refinement.

Nonlinearities may arise due to partial loss of contact, tread block impacts, or saturation effects in suspension components. While the reduced model is linear, it can be extended to include amplitude-dependent stiffness or clipping of displacement input. A simple extension is to allow k_t to depend on deflection magnitude or to introduce a nonlinear mapping from z_{eff} to F that saturates at high slopes. However, introducing nonlinearities complicates optimization and identification. Therefore, the initial focus is on geometries and operational regimes where linear approximation is reasonable, such as moderate amplitudes and smooth waveforms [29]. This is consistent with manufacturability and durability constraints that already discourage extreme shapes.

Finally, the validation strategy should consider perceptual relevance. Interior energy thresholds should correspond to detectable cues under realistic cabin noise. While the model uses weighted energy, the choice of weights and thresholds must be grounded. This can be done by mapping energy changes to estimated level changes in decibels relative to baseline in frequency bands of interest, using standard acoustic relationships. The aim is not to claim universal perceptual outcomes but to ensure that the constraint reflects plausible alerting increments.

By aligning calibration and validation with the model structure, one can build confidence that the optimization results correspond to real-world tradeoffs. The next section interprets the implications of the framework and examines the qualitative behavior of robustly optimized geometries.

6. Discussion and Implications

The proposed framework reframes road-edge profile design as spectral shaping under differential filtering [30]. This perspective clarifies why some geometries can reduce exterior noise without proportionally reducing interior alerting: the interior and exterior transfer paths emphasize different frequency bands and respond differently to tonal versus broadband excitation. A geometry that concentrates energy in bands where cabin transfer is strong but radiation efficiency is weak can maintain alerting while reducing far-field levels. Conversely, a geometry that excites strong tonal components in bands where outdoor propagation is efficient may generate disproportionate community impact, even if interior levels are only modestly increased.

One implication concerns the role of periodicity. Periodic geometries produce harmonic line spectra whose frequencies scale with speed. This can be beneficial for interior alerting if harmonics align with cabin resonances or with perceptually salient bands. However, periodicity also increases tonal prominence outside, which can elevate annoyance for residents even when average levels are moderate. The optimization framework captures this through weighting and optional tonal penalties, and it can recommend geometries that either soften periodicity by adding secondary components or that shift fundamental wavelengths so that dominant harmonics fall into less problematic exterior bands. In practice, this may correspond to smooth sinusoidal-like waveforms with carefully selected wavelengths and limited high-harmonic content, or to quasi-periodic waveforms that distribute energy [5].

Another implication concerns robustness to speed variability. Because the mapping from spatial frequency to temporal frequency is proportional to speed, the same geometry excites different temporal bands at different speeds. A design tuned narrowly to a single speed may fail to meet alerting constraints at lower speeds or may produce unexpected exterior peaks at higher speeds. Robust optimization naturally mitigates this by seeking geometries whose interior energy remains above threshold across the speed distribution. This tends to favor waveforms with energy spread across spatial frequencies so that, after speed scaling, some energy consistently lands in interior-favorable temporal bands. However, excessive broadband spatial content can increase exterior broadband noise, creating a tradeoff that must be bal-

anced.

Fleet heterogeneity introduces additional complexity. Vehicles with better cabin insulation may require stronger excitation to produce the same interior increment, while vehicles with stiffer suspensions may transmit more vibration and sound. A robust design should deliver alerting for insulated vehicles without producing extreme exterior noise for more transmissive vehicles [31]. The framework accommodates this by modeling transfer function distributions. The resulting design may not maximize alerting for any single vehicle but can achieve acceptable performance across the fleet. This is a typical feature of robust design: it sacrifices peak performance for reliability. In contexts where only a narrow vehicle class dominates, such as heavy trucks on a freight corridor, the uncertainty distribution can be specialized, yielding different design recommendations.

The role of the contact kernel $G(k)$ is also central. If G strongly attenuates high spatial frequencies, then attempting to shape fine geometric detail may be ineffective; the tire averages it out. This suggests that design effort should focus on spatial wavelengths that survive contact filtering. Moreover, because G depends on tire properties, uncertainty in contact patch length and compliance can blur the effect of higher spatial harmonics. Robust solutions thus often favor moderate spatial frequencies and smooth shapes, because these are less sensitive to contact variability [32]. This aligns with durability considerations, since smooth profiles also reduce stress concentrations.

From an agency perspective, the framework provides a mechanism to encode local priorities through weight functions and risk parameters. In a residential area, the exterior risk measure can be made more conservative by increasing β in CVaR or by emphasizing frequency bands that are more likely to penetrate buildings or be perceived as intrusive at night. In a high-speed rural corridor with sparse residences, the exterior objective can be relaxed, allowing designs that maximize alerting robustness. The same modeling and optimization tools can serve both contexts, enabling consistent decision logic rather than ad hoc changes.

The framework also suggests how to interpret field measurements beyond simple level comparisons. If a given geometry produces acceptable interior alerting but unexpected exterior noise, the model can diagnose whether the issue arises from radiation efficiency, propagation, or harmonic placement. For example, if exterior noise is dominated by a narrow band, that points toward periodic excitation and suggests adjusting wavelength or adding waveform components to redistribute energy. If exterior noise is broadband, that may indicate that the profile excites tire tread impacts or that the contact kernel differs from assumptions, perhaps due to wear or pavement texture [33]. Such diagnostics can inform maintenance and redesign decisions.

An important limitation is that the reduced model abstracts away many details of tire–road noise generation, including aerodynamic pumping in grooves, detailed tread block vibration, and nonlinear contact phenomena. While these details can matter for absolute prediction, the reduced model is intended primarily for comparative design and for capturing the main geometry-to-spectrum mapping. The validation strategy emphasizes fitting effective transfer functions, which can absorb some unmodeled physics. Nonetheless, there remains a risk of model-form error, particularly when geometries approach sharp-edged grooves or when operating conditions induce nonlinearities. This reinforces the role of field testing as a final verification stage and suggests that the optimization tool should be used to generate a small set of candidates rather than to declare a final design without validation.

The discussion also highlights an opportunity for extending the framework to multimodal alerting. Drivers respond not only to sound but also to steering wheel and seat vibration. A profile that produces strong low-frequency vibration may be effective even if cabin sound increases are modest, potentially allowing further exterior noise reduction [34]. Incorporating vibration explicitly would require defining a combined metric, perhaps based on band-weighted acceleration at the steering column and sound at the ear. The same contact force input can drive both, and the differential filtering argument becomes even more powerful because vibration and exterior sound are filtered by different pathways. Such an extension could yield designs that shift energy toward vibration-dominant bands and away from radiated sound bands, further improving the safety–noise tradeoff.

Another extension concerns spatial deployment strategy. Even if a profile is optimized, continuous installation near residences may still generate complaints due to repeated events. Agencies can consider targeted placement, such as limiting profiles to segments with higher departure risk or using variable geometry that changes along the corridor. The modeling framework can support such strategies by predicting how different geometries perform and by enabling designs tailored to specific risk zones. However, deployment strategy introduces behavioral and policy considerations beyond the present scope.

Overall, the framework provides a technical basis for rational geometry selection under competing objectives and uncertainty [35]. It emphasizes the idea that the safety function and noise externality are not inevitably coupled; rather, they can be decoupled through spectral shaping informed by physically grounded models and robust optimization.

7. Conclusion

This paper developed a coupled vibro-acoustic modeling and robust optimization framework for noise-constrained tactile warning infrastructure at the road edge. The central premise is that profile geometry influences interior alerting and exterior community noise through a structured spectral mapping: spatial geometry determines the temporal excitation spectrum via speed scaling and contact filtering, and that excitation is then shaped differently by vehicle cabin transfer functions and by acoustic radiation and propagation. By

making these pathways explicit in a reduced-order frequency-domain model, the framework enables geometry selection that exploits differential filtering to preserve interior salience while suppressing exterior impact.

The technical contributions include a compositional forward model linking profile spatial spectra to interior and exterior pressure spectra through contact kernels and transfer functions; a robust multi-objective formulation using risk measures that reflect reliability of interior alerting and conservatism against high-noise exterior events; and a surrogate-assisted solution strategy that accommodates manufacturability and durability constraints. A validation protocol was described to calibrate transfer functions and uncertainty models using field-reproducible measurements, emphasizing harmonization between interior and exterior metrics and generalization across vehicle classes and speeds.

The framework is intended as a design-stage tool that can narrow candidate geometries, clarify tradeoffs, and support context-specific tuning in noise-sensitive corridors without compromising safety function. Future technical work can extend the model to incorporate explicit vibration-based alerting metrics, refine radiation modeling for tonal prominence, and integrate deployment strategies that vary geometry along a corridor. By treating road-edge profiling as a controlled spectral design problem under uncertainty, agencies can move toward infrastructure solutions that are both safety-effective and community-compatible [36].

References

[1] D. J. Fonseca, G. P. Moynihan, and H. Fernandes, *The Role of Non-Recurring Congestion in Massive Hurricane Evacuation Events*, vol. 2011. InTech, 4 2011.

[2] A. K. Subedi, A. Rashidi, and N. Markovi, "Assessing roadside safety with computer vision: Fhwa ratings as the key predictor of rural road departure crashes and severity," *Journal of Advanced Transportation*, vol. 2025, 9 2025.

[3] L. K. Spainhour and A. Mishra, "Analysis of fatal run-off-the-road crashes involving overcorrection," *Transportation Research Record: Journal of the Transportation Research Board*, vol. 2069, pp. 1–8, 1 2008.

[4] O. Sallam, K. El-Rayes, E.-J. Ignacio, M. Al-Ghzawi, and R. Hajj, "Analyzing the effectiveness and external noise levels of sinusoidal and traditional shoulder rumble strips," *Transportation Research Record*, p. 03611981251400710, 2025.

[5] D. Horne, H. Jashami, C. M. Monsere, S. Kothuri, and D. S. Hurwitz, "Evaluating in-vehicle sound and vibration during incursions on sinusoidal rumble strips:," *Transportation Research Record: Journal of the Transportation Research Board*, vol. 2675, pp. 154–166, 12 2020.

[6] P. P. Jovanis and K.-F. Wu, "A cohort-based data structure design for analyzing crash risk using naturalistic driving data," in *Driving Assessment Conference 2013*, vol. 7, pp. 530–536, University of Iowa Libraries Publishing, 6 2013.

[7] V. S. Vinayaraj and V. Perumal, "Developing safety performance functions and crash modification factors for urban roundabouts in heterogeneous non-lane-based traffic conditions," *Transportation Research Record: Journal of the Transportation Research Board*, vol. 2677, pp. 644–661, 3 2023.

[8] B. K. Pathivada, A. Banerjee, K. Haleem, and T. Khan, "Developing safety performance functions for fatal and severe motorcycle crashes at intersections," *Transportation Research Record: Journal of the Transportation Research Board*, vol. 2679, pp. 373–387, 9 2025.

[9] J. S. Freeman, G. Watson, Y. E. Papelis, T. C. Lin, A. Tayyab, R. A. Romano, and J. G. Kuhl, "The iowa driving simulator: An implementation and application overview," in *SAE Technical Paper Series*, vol. 1, (United States), SAE International, 2 1995.

[10] Z. Li, M. Chitturi, A. R. Bill, and D. A. Noyce, "Automated identification and extraction of horizontal curve information from geographic information system roadway maps," *Transportation Research Record*, vol. 2291, pp. 80–92, 1 2012.

[11] M. B. Islam and A. Pande, "Analysis of single-vehicle roadway departure crashes on rural curved segments accounting for unobserved heterogeneity:," *Transportation Research Record: Journal of the Transportation Research Board*, vol. 2674, pp. 146–157, 8 2020.

[12] Q. A. Alomari, T. Y. Yosef, R. W. Bielenberg, R. K. Faller, M. Negahban, Z. Zhang, W. Li, and B. M. Humphrey, "Material characterization and stress-state-dependent failure criteria of aashto m180 guardrail steel: Experimental and numerical investigation.," *Materials (Basel, Switzerland)*, vol. 18, pp. 2523–2523, 5 2025.

[13] A. Solowczuk, *Effect of Bulb-outs at Intersections on Speed Reduction and Visibility Conditions in Tempo30 Zone*, pp. 24–34. Book Publisher International (a part of SCIENCEDOMAIN International), 6 2021.

[14] D. Nilsson, M. Lindman, T. Victor, and M. Dozza, "Definition of run-off-road crash clustersfor safety benefit estimation and driver assistance development," *Accident; analysis and prevention*, vol. 113, pp. 97–105, 3 2018.

[15] Z. Li, M. V. Chitturi, A. R. Bill, and D. A. Noyce, "Automated identification and extraction of horizontal curve information from geographic information system roadway maps," *Transportation Research Record: Journal of the Transportation Research Board*, vol. 2291, pp. 80–92, 1 2012.

[16] L. Hamilton, L. Humm, M. Daniels, and H. Yen, "The role of vision sensors in future intelligent vehicles," in

SAE Technical Paper Series, vol. 1, (United States), SAE International, 8 2001.

[17] S. C. Shindgikar, C. Chen, P.-S. Lin, Y. M. Keita, and E. Bialkowska-Jelinska, "Evaluating the safety effectiveness of edge line sinusoidal rumble strips on lane departure crashes prevention," *Transportation Research Record: Journal of the Transportation Research Board*, vol. 2679, pp. 236–251, 11 2024.

[18] D. L. Brien, "Forging continuing bonds from the dead to the living: Gothic commemorative practices along australias leichhardt highway," *M/C Journal*, vol. 17, 7 2014.

[19] T. Brown, J. D. Lee, and D. D. Fiorentino, "Effects of alcohol at 0.05alcohol concentration (bac) on low speed urban driving.," *Traffic injury prevention*, vol. 19, pp. S175–S177, 12 2018.

[20] E. S. Oguntade, S. S. Bako, and G. M. Mayaki, "On markovian modeling of vehicular traffic flow in gwagwalada metropolis, nigeria.," *Mathematika*, vol. 31, pp. 77–91, 7 2015.

[21] J. H. Everson, E. W. Kopala, L. E. Lazofson, H. C. Choe, and D. A. Pomerleau, "Sensor performance and weather effects modeling for intelligent transportation systems (its) applications," in *SPIE Proceedings*, vol. 2344, pp. 118–128, SPIE, 1 1995.

[22] Y.-S. Chen, J.-X. Liu, and Y.-F. Su, "Forward safety system using cameras with different focal lengths," in *SAE Technical Paper Series*, vol. 1, (United States), SAE International, 4 2012.

[23] "Parking slot prediction and face recognition based parked vehicle theft prevention in smart parking system," *International Research Journal of Modernization in Engineering Technology and Science*, 8 2024.

[24] F. Angioi, J. de Oña, C. Díaz-Piedra, R. de Oña, and L. L. D. Stasi, "Effectiveness of smart horizontal markings on drivers' behavior along horizontal curves: A driving simulation study.," *Accident; analysis and prevention*, vol. 219, pp. 108086–108086, 5 2025.

[25] M. R. R. Shaon, S. Zhao, K. Wang, and E. Jackson, "Developing a data-driven network screening procedure for systemic safety approach," *Transportation Research Record: Journal of the Transportation Research Board*, vol. 2678, pp. 348–364, 7 2023.

[26] E. R. Vaidogas, "Fragility of built urban objects to vicious attacks: Assessment by means of limited data on abnormal violent actions," *European Journal of Formal Sciences and Engineering*, vol. 5, pp. 16–29, 4 2022.

[27] N. P. Belz and L. Aultman-Hall, "Analyzing the effect of driver age on operating speed and acceleration noise: On-board second-by-second driving data," *Transportation Research Record: Journal of the Transportation Research Board*, vol. 2265, pp. 184–191, 1 2011.

[28] G. Ayres, B. H. Wilson, and J. LeBlanc, "Method for identifying vehicle movements for analysis of field operational test data," *Transportation Research Record*, vol. 1886, pp. 92–100, 1 2004.

[29] W. G. Najm, "Comparison of alternative crash avoidance sensor technologies," in *SPIE Proceedings*, vol. 2344, pp. 62–72, SPIE, 1 1995.

[30] E. Vergara, J. Aviles-Ordonez, Y. Xie, and M. Shirazi, "Understanding speeding behavior on interstate horizontal curves and ramps using networkwide probe data.," *Journal of safety research*, vol. 90, pp. 371–380, 6 2024.

[31] K. H. DeCarlo, T. Thomas, and J. Wielinski, "Impact of rumble strips on longitudinal joint pavement performance," *Transportation Research Record: Journal of the Transportation Research Board*, vol. 2677, pp. 766–776, 4 2023.

[32] T. Redmon and C. Zegeer, "In step with safety," *Public roads*, vol. 70, pp. 2–7, 9 2006.

[33] W. D. Bachalo, A. S. Inenaga, and C. A. Schuler, "Advanced laser based tracking device for motor vehicle lane position monitoring and steering assistance," *SPIE Proceedings*, vol. 2592, pp. 128–137, 12 1995.

[34] J. A. Misener, C. Thorpe, R. Ferlis, R. Hearne, M. Siegal, and J. Perkowski, "Sensor-friendly vehicle and roadway cooperative safety systems: Benefits estimation," *Transportation Research Record: Journal of the Transportation Research Board*, vol. 1746, pp. 22–29, 1 2001.

[35] V. K. Narendran, D. B. Pape, J. A. Hadden, J. H. Everson, and D. A. Pomerleau, "Analytical methodology for design and performance assessment of run-off-road collision avoidance systems," in *SAE Technical Paper Series*, vol. 1, (United States), SAE International, 2 1997.

[36] T. Y. Liao and R. B. Machemehl, "Development of an aggregate fuel consumption model for signalized intersections," *Transportation Research Record*, vol. 1641, pp. 9–18, 1 1998.